

Error-Tolerant Geometric Quantum Control for Logical Qubits with Minimal Resource

Tao Chen,^{1,2} Zheng-Yuan Xue,^{2,3,*} and Z. D. Wang^{1,3,†}

¹*Guangdong-Hong Kong Joint Laboratory of Quantum Matter, Department of Physics, and HKU-UCAS Joint Institute for Theoretical and Computational Physics at Hong Kong, The University of Hong Kong, Pokfulam Road, Hong Kong, China*

²*Guangdong Provincial Key Laboratory of Quantum Engineering and Quantum Materials, and School of Physics and Telecommunication Engineering, South China Normal University, Guangzhou 510006, China*

³*Guangdong-Hong Kong Joint Laboratory of Quantum Matter, and Frontier Research Institute for Physics, South China Normal University, Guangzhou 510006, China*

(Dated: December 17, 2021)

Geometric quantum computation offers a practical strategy toward robust quantum computation due to its inherently error tolerance. However, the rigorous geometric conditions lead to complex and/or error-disturbed quantum controls, especially for logical qubits that involve more physical qubits, whose error tolerance is effective in principle though, their experimental demonstration is still demanding. Thus, how to best simplify the needed control and manifest its full advantage has become the key to widespread applications of geometric quantum computation. Here we propose a new fast and robust geometric scheme, with the decoherence-free-subspace encoding, and present its physical implementation on superconducting quantum circuits, where we only utilize the experimentally demonstrated parametrically tunable coupling to achieve high-fidelity geometric control over logical qubits. Numerical simulation verifies that it can efficiently combine the error tolerance from both the geometric phase and logical-qubit encoding, displaying our gate-performance superiority over the conventional dynamical one without encoding, in terms of both gate fidelity and robustness. Therefore, our scheme can consolidate both error suppression methods for logical-qubit control, which sheds light on the future large-scale quantum computation.

I. INTRODUCTION

The superiority of quantum computation over classical one essentially lies in the superposition and entanglement of quantum systems [1]. But an inescapable truth is that, the effects of the environment-induced decoherence and inaccurate control on a quantum system will greatly limit the performance of quantum gates, which are the building blocks for executing quantum computation, thus revealing the necessity for exploring a method to combat both decoherence and control errors, especially for future large-scale quantum circuits. Geometric phases [2–5], due to their inherent error-tolerant feature, have become critical elements for realizing high-fidelity and robust quantum controls. However, for adiabatic geometric quantum computation (GQC) [6–10], due to long evolution time needed to satisfy the adiabatic conditions, the resulting gate fidelities are relatively low, despite they are indeed being more robust against control errors.

Recently, GQC [11–17] based on the nonadiabatic geometric phases [4, 5] have been proposed to implement robust and high-fidelity quantum gates, which eliminate the restriction of slow evolution. Remarkably, experimental demonstrations for elementary geometric quantum gates have also been achieved on various systems, such as trapped ions [18, 19], NMR [20–23], superconducting quantum circuits [24–30], and nitrogen vacancy centers [31–36], etc. Meanwhile, to further consolidate the geometric robustness, many efforts have been made to make GQC being compatible with various optimal-control techniques, including the composite pulse [37, 38], dynamical

decoupling [39, 40], time-optimal control [41], path optimization [42], etc. Nonetheless, the rigorous geometric conditions lead to complex and error-disturbed quantum controls, so that existing GQC is favourable merely for a certain kind of control error. Thus, it is still quite challenging to demonstrate the full error-tolerant advantages for GQC.

Besides the control errors, the environmental induced decoherence is another central obstacle in realizing GQC. To this end, the proposed geometric schemes [43–50] under the protection of decoherence-free-subspace (DFS) encoding [51–54] aim to achieve the combination of the geometric error-tolerant features and decoherence resilience of the encoding. However, due to more involved physical qubits, more error sources are introduced too, such that the logical-qubit manipulation becomes complicated and fail to achieve better gate performance under their hybrid protection in subsequent experimental demonstration.

Here we aim to solve the two aforementioned key problems in GQC: (i) to best simplify the geometric quantum control that manifests full advantage of GQC; (ii) to make GQC more compatible with the protection of DFS encoding. To this end, from a general approach to construct geometric quantum gate, we propose a new geometric scheme that can shorten the operation time and possess the robustness advantage beyond the conventional dynamical scheme. In addition, with the pursuit of a minimal number of physical qubits, we merely utilize parametrically tunable coupling between a transmon and a microwave resonator to achieve high-fidelity geometric control for DFS logical qubits on superconducting quantum circuit. Our scheme does not need additional auxiliary level/qubit, and thus avoids introducing more error sources. Numerical simulation verifies that our scheme can fully consolidate the hybrid-protection capabilities from both geometric phase and

* zyxue83@163.com

† zwang@hku.hk

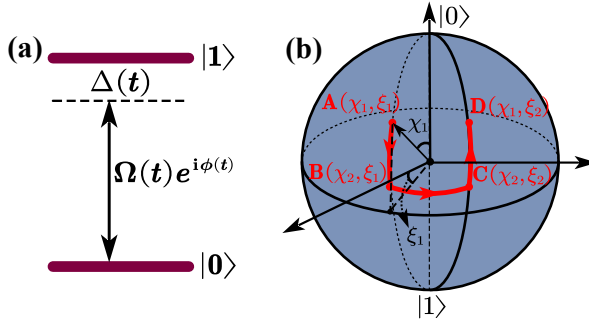


FIG. 1. (a) A simple two-level coupling structure driven by a microwave field. (b) Illustration of the evolution path $\mathbf{A} \rightarrow \mathbf{B} \rightarrow \mathbf{C} \rightarrow \mathbf{D}$ of state $|\Psi_0(t)\rangle$ on a Bloch sphere.

the encoding, by displaying absolute error-tolerant advantages over the dynamical gates without encoding, in terms of both frequency-drift error and decoherence, which are the main error source for superconducting quantum circuits. Therefore, our scheme shows the prospect of GQC with logical-qubit encoding that is inevitable in future fault-tolerant quantum computation.

II. A GENERAL SCHEME FOR GEOMETRIC GATES

We first consider a general two-level quantum system that consists of a ground state $|0\rangle = (1, 0)^\dagger$ and an excited state $|1\rangle = (0, 1)^\dagger$, as shown in Fig. 1(a). Its arbitrary quantum control can be realized by a microwave drive, as described by the Hamiltonian of

$$\mathcal{H}(t) = \frac{1}{2} \mathbf{B}(t) \cdot \boldsymbol{\sigma}, \quad (1)$$

where control field $\mathbf{B}(t)$ has three directions, which are $B_x = \Omega(t) \cos \phi(t)$, $B_y = \Omega(t) \sin \phi(t)$ and $B_z = -\Delta(t)$, respectively; $\boldsymbol{\sigma} = (\sigma_x, \sigma_y, \sigma_z)$ are the Pauli matrices; $\Omega(t)$ and $\phi(t)$ are the time-dependent driving amplitude and phase of the microwave field, and $\Delta(t)$ is the time-dependent detuning. There is a pair of orthogonal evolution states $|\Psi_i(t)\rangle = e^{i f_i(t)} |\psi_i(t)\rangle$ with subscript $i=0, 1$, $|\psi_0(t)\rangle = \cos \frac{\chi(t)}{2} |0\rangle + \sin \frac{\chi(t)}{2} e^{i \xi(t)} |1\rangle$ and $|\psi_1(t)\rangle = \sin \frac{\chi(t)}{2} e^{-i \xi(t)} |0\rangle - \cos \frac{\chi(t)}{2} |1\rangle$, where the phase factor $f_i(t)$ is a global phase of $|\Psi_i(t)\rangle$, $\chi(t)$ and $\xi(t)$ represent the time-dependent change of polar and azimuth angles of the state vector on a Bloch sphere, as shown in Fig. 1(b). Utilizing the Schrödinger equation as $i|\dot{\Psi}_i(t)\rangle = \mathcal{H}(t)|\Psi_i(t)\rangle$, we solve for

$$\begin{aligned} \dot{\chi}(t) &= -B_x \sin \xi(t) + B_y \cos \xi(t), \\ \dot{\xi}(t) &= -\Delta(t) - \cot \chi(t) [B_x \cos \xi(t) + B_y \sin \xi(t)], \end{aligned} \quad (2)$$

thereby determining the dependence of evolution details of state $|\Psi_i(t)\rangle$ and the control parameters of $\mathcal{H}(t)$. Besides, after a time period τ , accumulated global phase $f_0(\tau) = -f_1(\tau) = \gamma$ includes the dynamical part $\gamma_d = -\int_0^\tau \langle \Psi_i(t) | \mathcal{H}(t) | \Psi_i(t) \rangle dt$ and the geometric part

$$\gamma_g = \gamma - \gamma_d = -\frac{1}{2} \int_0^\tau \dot{\xi}(t) [1 - \cos \chi(t)] dt, \quad (3)$$

where the geometric nature [4, 5] of γ_g comes from the fact that it is given by half of the solid angle enclosed by the non-cyclic evolution path and its geodesic connecting the initial point $[\chi(0), \xi(0)]$ and the final point $[\chi(\tau), \xi(\tau)]$. In this way, we can determine the pure geometric property of the evolution process by designing state parameters $\xi(t) \sin^2 \chi(t) = -\Delta(t)$ to meet $\gamma_d = 0$. Thus, submitting this geometric condition into Eq. (2), we can use the following relations

$$\begin{aligned} B_x &= -\dot{\xi}(t) \sin \chi(t) \cos \chi(t) \cos \xi(t) - \dot{\chi}(t) \sin \xi(t), \\ B_y &= -\dot{\xi}(t) \sin \chi(t) \cos \chi(t) \sin \xi(t) + \dot{\chi}(t) \cos \xi(t), \\ B_z &= -\dot{\xi}(t) \sin^2 \chi(t), \end{aligned} \quad (4)$$

to reversely fix the control parameters of Hamiltonian $\mathcal{H}(t)$.

After an evolution period τ , two evolution states undergo a change as $|\Psi_i(0)\rangle \rightarrow |\Psi_i(\tau)\rangle = e^{(-1)^i i \gamma_g} |\psi_i(t)\rangle$, the associated evolution operator

$$\begin{aligned} U(\tau, 0) &= e^{i\gamma} |\psi_0(0)\rangle \langle \psi_0(0)| + e^{-i\gamma} |\psi_1(0)\rangle \langle \psi_1(0)| \quad (5) \\ &= \begin{pmatrix} (c_{\gamma'} c_{\chi_-} + i s_{\gamma'} s_{\chi_+}) e^{-i\xi_-} & (-c_{\gamma'} s_{\chi_-} + i s_{\gamma'} s_{\chi_+}) e^{-i\xi_+} \\ (c_{\gamma'} s_{\chi_-} + i s_{\gamma'} s_{\chi_+}) e^{i\xi_+} & (c_{\gamma'} c_{\chi_-} - i s_{\gamma'} s_{\chi_+}) e^{i\xi_-} \end{pmatrix}, \end{aligned}$$

can be obtained, where $c_j = \cos j$, $s_j = \sin j$, $p_\pm = [p(\tau) \pm p(0)]/2$ and $\gamma' = \gamma_g + \xi_-$. Thus, arbitrary geometric gates are realized by setting boundary value of $\chi(t)$ and $\xi(t)$.

III. A NEW CONSTRUCTION OF GEOMETRIC GATES

In the above general geometric framework, we can also set time-dependent shapes of parameters $\chi(t)$ and $\xi(t)$ to realize different geometric evolution processes. We here design a new geometric evolution scheme with state parameters $(\chi(t), \xi(t))$ as follows:

$$\begin{aligned} \chi(0) &= \chi_1 \rightsquigarrow \chi(\tau_1) = \chi_2 \rightarrow \chi(\tau_2) = \chi_2 \rightsquigarrow \chi(\tau) = \chi_1 \\ \xi(0) &= \xi_1 \rightarrow \xi(\tau_1) = \xi_1 \rightsquigarrow \xi(\tau_2) = \xi_2 \rightarrow \xi(\tau) = \xi_2 \end{aligned} \quad (6)$$

where arrows “ \rightarrow ” and “ \rightsquigarrow ” indicate whether the parameters $\chi(t)$ and $\xi(t)$ remain constant or change with time during the evolution process, respectively. For example, in the first time segment $t \in [0, \tau_1]$, $\chi(t)$ changes from χ_1 to χ_2 , while $\xi(t) = \xi_1$ remains constant. The visualized state-evolution details on a Bloch sphere are shown in Fig. 1(b), that is: start from point $\mathbf{A}(\chi_1, \xi_1)$ and evolve along the longitude line with $\xi(t) = \xi_1$ to point $\mathbf{B}(\chi_2, \xi_1)$ at the time τ_1 ; then evolve along the latitude line with $\chi(t) = \chi_2$ to point $\mathbf{C}(\chi_2, \xi_2)$ at the time τ_2 ; finally evolve to point $\mathbf{D}(\chi_1, \xi_2)$ along the longitude line with $\xi(t) = \xi_2$ at the final time τ . Therefore, under the above evolution process, according to the parameter-limited relation in Eq. (4), we can determine the Hamiltonian parameters $\Omega(t)$ and $\phi(t)$ in these three segments $t \in [0, \tau_1]$, $[\tau_1, \tau_2]$ and $[\tau_2, \tau]$ as

$$\begin{aligned} \int_0^{\tau_1} \Omega(t) dt &= |\chi_2 - \chi_1|, & \phi(t) &= \xi_1 + \frac{\pi}{2}, \\ \int_{\tau_1}^{\tau_2} \Omega(t) dt &= 2(\xi_2 - \xi_1) \sin(2\chi_2), & \phi(t) &= \xi(t) + \pi, \\ \int_{\tau_2}^{\tau} \Omega(t) dt &= |\chi_2 - \chi_1|, & \phi(t) &= \xi_2 - \frac{\pi}{2}, \end{aligned} \quad (7)$$

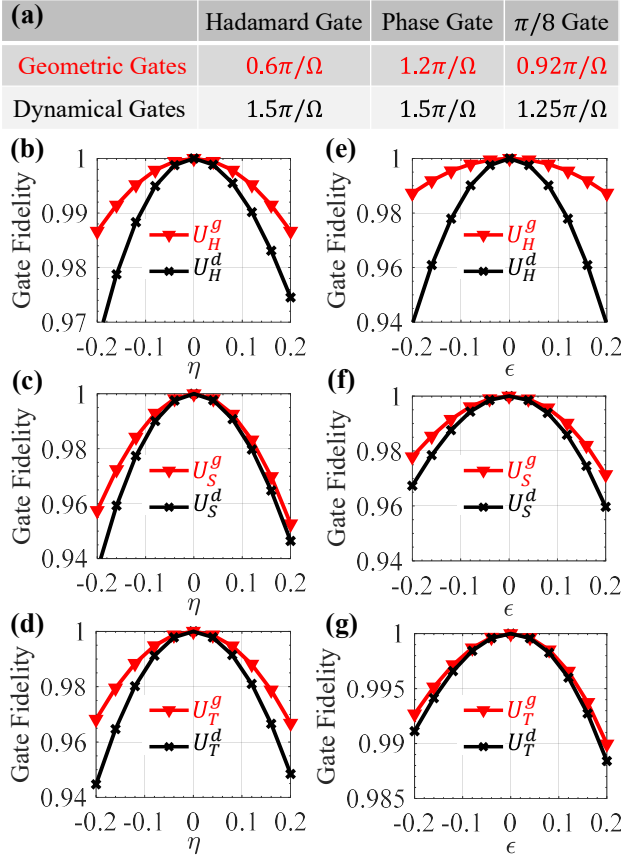


FIG. 2. Comparison of our geometric gates and the conventional dynamical counterparts in terms of (a) gate time and (b)-(g) robustness.

respectively, with detuning $\Delta(t) = 0, -\Omega(t) \tan \chi_2, 0$, where $\xi(t) = \xi_1 + \int_{\tau_1}^t \Omega(t') dt' / [2 \sin(2\chi_2)]$. This is the case of $\chi_2 > \chi_1$, and when $\chi_2 < \chi_1$, parameter $\phi(t)$ in the time segments $t \in [0, \tau_1]$ and $t \in [\tau_2, \tau]$ should be changed to $\xi_1 - \pi/2$ and $\xi_2 + \pi/2$, respectively. Notice that, the pulse shape here can be arbitrary, providing their pulse area are as prescribed. The final evolution operator is written as

$$U(\tau) = U(\tau, \tau_2)U(\tau_2, \tau_1)U(\tau_1, 0) \quad (8)$$

$$= \begin{pmatrix} (c_{\gamma'} + i s_{\gamma'} c_{\chi_1}) e^{-i\xi_-} & i s_{\gamma'} s_{\chi_1} e^{-i\xi_+} \\ i s_{\gamma'} s_{\chi_1} e^{i\xi_+} & (c_{\gamma'} - i s_{\gamma'} c_{\chi_1}) e^{i\xi_-} \end{pmatrix},$$

where $\gamma' = \gamma_g + \xi_-$ with the accumulated geometric phase in this evolution process being $\gamma_g = -(\xi_2 - \xi_1)(1 - \cos \chi_2)/2$. We find that geometric Hadamard gate U_H^g , Phase gate U_S^g and $8/\pi$ gate U_T^g can be realized by setting $\{\gamma' = \pi/4, \xi_2 - \xi_1 = 3\pi, \chi_1 = \pi/2\}$, $\{\gamma' = \pi, \xi_2 - \xi_1 = 5\pi/2\}$ and $\{\gamma' = \pi, \xi_2 - \xi_1 = 9\pi/4\}$, which constitute a universal set for single-qubit gates.

IV. THE PERFORMANCE SUPERIORITY OF GEOMETRIC GATES

Next, we continue to verify the advantages of our new geometric scheme over the conventional dynamical one (for details, see Appendix A), in terms of gate performance. Firstly,

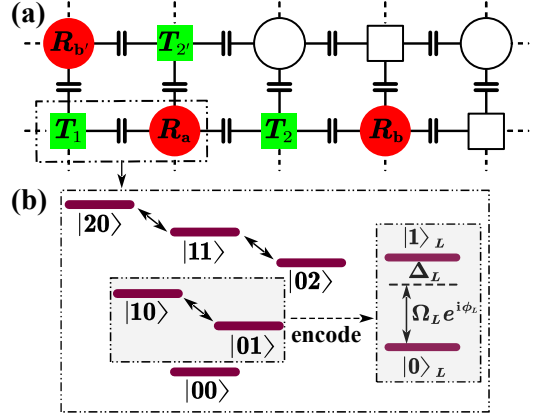


FIG. 3. (a) A scalable 2D superconducting transmon-resonator lattice. (b) Energy level diagram of the capacitive coupling of a single transmon and a microwave resonator, where the single-excitation subspace $\{|10\rangle, |01\rangle\}$ as an effective two-level structure can encode a single-logical-qubit DFS.

the needed gate-operation time is an important factor for gate performance, determines the impacts from environment-induced decoherence. From the comparison results are listed in Fig. 2(a), we can find that the time we consume to construct geometric gate is less than that of the dynamical counterpart, where $\Omega(t) = \Omega$ is set to be constant for simplicity. Secondly, we also consider the driving amplitude and detuning errors induced by the imperfect control, in the form of $(1 + \epsilon)\Omega$ and $\Delta(t) + \eta\Omega$. We use the formula $F_{\epsilon, \eta} = \text{Tr}(U^\dagger U_{\epsilon, \eta}) / \text{Tr}(U^\dagger U)$ to evaluate gate robustness in the presence of control errors, in which U and $U_{\epsilon, \eta}$ are, respectively, the gate without and with error. The results of numerical simulation are shown in Figs. 2(b)-2(g), which exhibit the advantage of our scheme in terms of both gate fidelity and robustness.

V. IMPLEMENTATION WITH ENCODING

For the superconducting transmon qubit, the precise control of a single qubit, a common method is to apply the DRAG correction technology [55, 56] to suppress the computational basis leakage caused by the transmon's anharmonicity. However, it is necessary to set the drive to be time-dependent there, resulting in a longer gate time than the square pulse, so the decoherence effect and loss of gate robustness will also increase significantly. Therefore, we here propose to implement our universal geometric gates under the protection of DFS encoding on a two-dimensional (2D) transmon-resonator lattice as shown in Fig. 3(a), which can combine error-tolerant features of our geometric scheme and decoherence resilience of DFS encoding. With the pursuit of a minimal number of physical qubits and without any additional auxiliary, we here only use capacitively coupled transmon T_1 and microwave resonator R_a to encode a DFS logical qubit, thus there will exist a two-dimensional DFS $S_1 = \{|10\rangle, |01\rangle\}$, where the encoded computational basis are denoted as $|0\rangle_L = |10\rangle$ and $|1\rangle_L = |01\rangle$ with $|mn\rangle = |m\rangle_1 \otimes |n\rangle_a$. For the parametrically tunable cou-

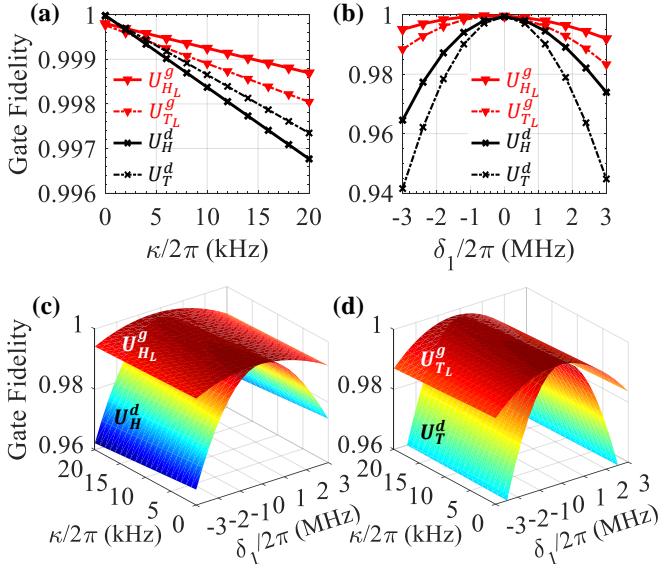


FIG. 4. Under the effects of (a) decoherence and (b) qubit-frequency drift which are regard as the main source of gate errors in the superconducting quantum circuits, the performance comparison for our geometric gates under the protection of DFS encoding and the dynamical gates realized on a single transmon. Comparison of comprehensive effects for (c) Hadamard gate and (d) $\pi/8$ gate. Note that the performance of the Phase gate is similar to that of its same type of $\pi/8$ gate and thus not mention here and hereafter.

pling [57, 58] between a transmon T_1 and a fixed-frequency microwave resonator R_a , it is obtained by introducing an additional qubit-frequency driving for transmon T_1 , in the form of $\omega_{q_1}(t) = \omega_{q_1} + \varepsilon_1 \sin(\nu_1 t + \varphi_1)$, which can be experimentally achieved by biasing the transmon with an ac magnetic flux. Energy level transition structure of the above interaction Hamiltonian as shown in Fig. 3(b), there is naturally no leakage from DFS S_1 to the multi-excitation subspaces, thus no additional correction for the computational basis leakage is required. Furthermore, in the DFS representation $\{|0\rangle_L, |1\rangle_L\}$, the obtained effective Hamiltonian is of the same form as Eq. (1) (for the derivation details, see Appendix B), thus arbitrary single-logical-qubit geometric gates, as in Eq. (8), can be realized under the geometric parameter constraints in Eq. (7).

We take Hadamard gate $U_{H_L}^g$, Phase gate $U_{S_L}^g$ and $\pi/8$ gate $U_{T_L}^g$ as typical examples to numerically show the performance of these universal single-logical-qubit geometric gates by using the quantum master equation, where the simulation details are seen in Appendix D. According to the state-of-the-art technology in the experiments [59, 60], we here set decoherence rates $\kappa_1 = \kappa_z = \kappa = 2\pi \times 4$ kHz, $\kappa_a = 2\pi \times 1$ kHz, and the coupling strength between transmon T_1 and microwave resonator R_a to $g_{1a} = 2\pi \times 20$ MHz with anharmonicity of transmon T_1 as $\alpha_1 = 2\pi \times 240$ MHz. At frequency difference between T_1 and R_a as $\Delta_1 = 2\pi \times 180$ MHz, the gate fidelities of geometric Hadamard gate, Phase gate and $\pi/8$ gate can be as high as 99.95%, 99.92% and 99.94% by adjusting $\beta_1 = \frac{\varepsilon_1}{\nu_1} \approx 2.1$, respectively. Besides, for superconducting quantum circuits, the frequency drift ($\omega_{q_1} \rightarrow \omega_{q_1} + \delta_1$) of a working transmon

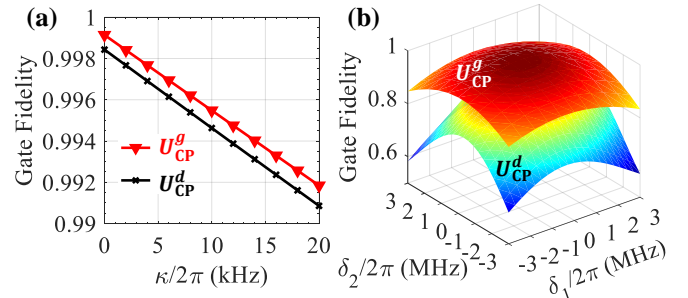


FIG. 5. Under the effects of (a) decoherence and (b) qubit-frequency drifts ($\omega_{q_1} \rightarrow \omega_{q_1} + \delta_1$ and $\omega_{q_2} \rightarrow \omega_{q_2} + \delta_2$) of transmons T_1 and T_2 , the performance comparison for two-logical-qubit controlled-phase geometric gate and two-physical-qubit dynamical counterpart.

can up to a few of MHz. In Figs. 4(a) and 4(b), we plot the gate fidelities as functions of κ and δ_1 , these results demonstrate that, although more physical resources are involved, our encoding scheme can still has a stronger robustness than the conventional dynamical gates, which are realized by applying DRAG correction on a single transmon (T_1) under the same parameter settings. Remarkably, we consider both key errors, as shown in Figs. 4(c) and 4(d), which can further verify error-tolerant features of our scheme.

Next, we extend our geometric approach to the situation of two logical qubits, as shown in Fig. 3(a), and prove the overall gate-performance advantages compared to “two-physical-qubit dynamical gate” realized by tunable coupling between only two transmons. We continue to utilize a transmon T_2 and a microwave resonator R_b on the same chain as the first logical qubit to encode the second logical qubit, thus there exists a four-dimensional DFS $S_2 = \{|1010\rangle, |1001\rangle, |0110\rangle, |0101\rangle\} = \{|00\rangle_L, |01\rangle_L, |10\rangle_L, |11\rangle_L\}$ for two-logical qubits. In a same way, the derivation details as seen in Appendix C, we can efficiently obtain two-logical-qubit controlled-phase gate

$$U_{CP}^g(\zeta) = \text{diag}\{1, 1, e^{i\zeta}, 1\}, \quad (9)$$

with ζ being a geometric phase. In the following, we evaluate the performance of $U_{CP}^g(\pi/2)$ by utilizing the master equation, in which the effects of high-order oscillating terms and decoherence of transmons (T_1, T_2) and microwave resonators (R_a, R_b) are all taken into consideration. Here, we set the coupling strength $g_{a2} = 2\pi \times 8$ MHz, and anharmonicity of the other transmon T_2 as $\alpha_2 = 2\pi \times 220$ MHz. When frequency difference between T_2 and R_a as $\Delta_2 = 2\pi \times 500$ MHz and driving parameter $\beta_2 = \frac{\varepsilon_2}{\nu_2} \approx 1.2$, we can simulate that the fidelity of two-logical-qubit controlled-phase geometric gate can up to 99.76% under the decoherence rates $\kappa = 2\pi \times 4$ kHz and $\kappa_a = \kappa_b = 2\pi \times 1$ kHz, which is comparable to the fidelity with 99.68% of two-physical-qubit dynamical one $U_{CP}^d(\pi/2)$ realized only on transmons T_1 and T_2 under the same parameter settings. Furthermore, in Figs. 5(a) and 5(b), the numerical results indicate that our controlled-phase geometric gate shows a stronger error-tolerant feature over the two-physical-qubit dynamical gate.

VI. CONCLUSION

In summary, we have proposed a fast and robust geometric scheme based on a simple two-level structure. And we merely utilize tunable coupling between a transmon and a microwave resonator to achieve high-fidelity geometric logical control in superconducting quantum circuits. Furthermore, from the numerical results, we can obviously find that, under hybrid protection of geometric phase and DFS encoding, our single- and two-logical-qubit geometric gates can all show higher fidelity and greater robustness than the dynamical ones without DFS encoding. Therefore, all of these sufficiently demonstrate that our scheme paves the way for achieving the robust GQC.

ACKNOWLEDGMENTS

The authors thank Z. Hua and S. Li for helpful discussions. This work was supported by the Key-Area Research and Development Program of GuangDong Province (Grant No. 2019B030330001), the CRF (No. C6009-20G) of Hong Kong, the National Natural Science Foundation of China (Grant No. 11874156), and Science and Technology Program of Guangzhou (Grant No. 2019050001).

Appendix A: Dynamical quantum gates

Conventional dynamical quantum gate [60, 61], mentioned in the main text, can be realized by a resonant two-level drive. The corresponding Hamiltonian is as Eq. (1) with $\Delta(t) = 0$, in which driving phase $\phi(t) = \phi_d$ is a constant to ensure that there is no accumulation of geometric phase. In this way, dynamical Hadamard gate U_H^d , Phase gate U_S^d and $8/\pi$ gate U_T^d are, respectively, obtained by the operations of $R_x(\pi)R_y(\frac{\pi}{2})$, $R_y(-\frac{\pi}{2})R_x(\frac{\pi}{2})R_y(\frac{\pi}{2})$ and $R_y(-\frac{\pi}{2})R_x(\frac{\pi}{4})R_y(\frac{\pi}{2})$, where the corresponding operation elements $R_x(\theta)$ and $R_y(\theta)$ are the dynamical X- and Y-axis rotation operations for arbitrary angle $\theta = \int_0^T \Omega(t)dt$, which can be done by determining $\phi_d = 0$ and $\pi/2$, respectively.

In addition, in the superconducting physical implementation of single-qubit dynamical gates, the corresponding control field needs to be corrected to $\mathbf{B}_C(t) = \mathbf{B}(t) + \mathbf{B}_D(t)$, in which $\mathbf{B}(t)$ and $\mathbf{B}_D(t) = (-\dot{B}_y + B_z B_x, \dot{B}_x + B_z B_y, 0)/(2\alpha_1)$ are the original and additional DRAG-correcting microwave fields, respectively, where α_1 is anharmonicity of the working transmon T_1 . Consider the constraints of experimental control and DRAG correction on a single transmon, it is necessary to set a time-dependent pulse shape and ensure $\Omega(0) = \Omega(\tau) = 0$. In the comparison of main text, we take $\Omega(t) = \Omega_m \sin(\pi t/\tau)$ as an example for simplicity.

Appendix B: Tunable transmon-resonator coupling

To achieve effective control for the single-logical-qubit states $|0\rangle_L$ ($|10\rangle$) and $|1\rangle_L$ ($|01\rangle$), we can utilize the paramet-

rically tunable coupling between a transmon T_1 and a fixed-frequency microwave resonator R_a , which is obtained by introducing an additional qubit-frequency driving for transmon T_1 . Move into the interaction picture, the system Hamiltonian can be written as

$$\begin{aligned} \mathcal{H}_I^1(t) = g_{1a} & \left\{ |10\rangle\langle 01|e^{i\Delta_1 t}e^{-i\beta_1 \cos(\nu_1 t + \varphi_1)} \right. \\ & + \sqrt{2}|20\rangle\langle 11|e^{i(\Delta_1 - \alpha_1)t}e^{-i\beta_1 \cos(\nu_1 t + \varphi_1)} \\ & \left. + \sqrt{2}|11\rangle\langle 02|e^{i\Delta_1 t}e^{-i\beta_1 \cos(\nu_1 t + \varphi_1)} \right\} + \text{H.c.}, \end{aligned} \quad (S1)$$

where $\beta_1 = \varepsilon_1/\nu_1$; g_{1a} and Δ_1 are coupling strength and the difference of the transition frequency between transmon T_1 and microwave resonator R_a ; α_1 is the intrinsic anharmonicity of transmon T_1 . The energy level transition structure corresponding to the Hamiltonian $\mathcal{H}_I^1(t)$ as shown in Fig. 3(b), we obviously find that the single-excitation subspace $\{|10\rangle, |01\rangle\}$ can form an effective two-level structure. Furthermore, when we encode the computational basis into DFS S_1 , there is naturally no leakage from S_1 to the multi-excitation subspaces. Therefore, unlike the control in a single transmon, our encoding method is not limited by the transmon's anharmonicity, and also does not rely strictly on a time-dependent pulse shape for correcting the computational basis leakage.

We here utilize the Jacobi-Anger identity to expand e-index terms in Eq. (S1), and modulate the qubit-driving frequency ν_1 to satisfy $\Delta_1 - \nu_1 = -(\Delta_L + \mu)$ with $|\Delta_L + \mu| \ll \{\Delta_1, \nu_1\}$. Then, by neglecting the high-order oscillating terms, and applying the unitary transformation with the transformation matrix $U_R(t) = \exp[-i(\Delta_L/2)\sigma_z^L t]$, the final effective Hamiltonian can be obtained as

$$\mathcal{H}_L(t) = \frac{1}{2}\Omega_L[\cos\phi_L(t)\sigma_x^L + \sin\phi_L(t)\sigma_y^L] - \frac{1}{2}\Delta_L\sigma_z^L, \quad (S2)$$

where $\sigma_{x,y,z}^L$ are the Pauli operators in the single-logical-qubit subspace $\{|0\rangle_L, |1\rangle_L\}$; the coupling strength $\Omega_L = 2J_1(\beta_1)g_{1a}$ with $J_1(\beta_1)$ being a Bessel function of the first kind, and the relative phase $\phi_L(t) = \mu t + \varphi_1 + \pi/2$. The above Hamiltonian form is equivalent to $\mathcal{H}(t)$ of Eq. (1) under the DFS representation $\{|0\rangle_L, |1\rangle_L\}$.

Appendix C: Two-logical-qubit geometric gate

As shown in Fig. 3(a), we continue to utilize another transmon T_2 and a resonator R_b on the same chain as the first logical qubit to encode the second logical qubit. With the general scalability of our encoding scheme, we can also utilize $T_{2'}$ and $R_{b'}$ in the column direction of two-dimensional superconducting lattice to encode the second logical qubit. In addition, for the arbitrary target control of the two-logical-qubit states, we can realize it by the parametrically tunable coupling between adjacent microwave resonator R_a and transmon T_2 , in which transmon T_2 is driven by an additional qubit-frequency driving in the form of $\omega_{q_2}(t) = \omega_{q_2} + \varepsilon_2 \sin(\nu_2 t + \varphi_2)$. Thus, the

corresponding interaction Hamiltonian can be described as

$$\begin{aligned} \mathcal{H}_I^2(t) = & g_{a2} \left\{ |01\rangle_{a2}\langle 10| e^{i\Delta_2 t} e^{-i\beta_2 \cos(\nu_2 t + \varphi_2)} \right. \\ & + \sqrt{2} |02\rangle_{a2}\langle 11| e^{i(\Delta_2 - \alpha_2)t} e^{-i\beta_2 \cos(\nu_2 t + \varphi_2)} \\ & \left. + \sqrt{2} |11\rangle_{a2}\langle 20| e^{i\Delta_2 t} e^{-i\beta_2 \cos(\nu_2 t + \varphi_2)} \right\} + \text{H.c.}, \end{aligned} \quad (\text{S3})$$

where $\beta_2 = \varepsilon_2/\nu_2$; g_{a2} and Δ_2 are coupling strength and the difference of the transition frequency between transmon T_2 and microwave resonator R_a . Energy level transition structure of the Hamiltonian $\mathcal{H}_I^2(t)$ is similar to Fig. 3(b). But, different from the single-logical-qubit case manipulated in the single-excitation subspace, the manipulation of our two-logical-qubit states need to be implemented in the two-excitation subspace $\{|02\rangle_{a2}, |11\rangle_{a2}\}$ to realize a nontrivial controlled-phase gate. To this end, we here modulate driving frequency ν_2 to satisfy $\Delta_2 - \alpha_2 - \nu_2 = -(\Delta_{L_2} + v)$ with $|\Delta_{L_2} + v| \ll \{\Delta_2 - \alpha_3, \nu_2\}$, and apply the unitary transformation, the Hamiltonian mapped into the DFS S_2 representation can then read as

$$\begin{aligned} \mathcal{H}_{L_2}(t) = & -\frac{\Delta_{L_2}}{2} (|a\rangle_L \langle a| - |11\rangle_L \langle 11|) \\ & + \frac{\Omega_{L_2}}{2} (e^{-i\phi_{L_2}(t)} |a\rangle_L \langle 11| + \text{H.c.}), \end{aligned} \quad (\text{S4})$$

where the auxiliary state $|a\rangle_L = |0020\rangle$, and the effective coupling strength and relative phase are $\Omega_{L_2} = 2\sqrt{2}J_1(\beta_2)g_{a2}$ and $\phi_{L_2}(t) = vt + \varphi_2 + \pi/2$, respectively. For a set of orthogonal evolution states

$$\begin{aligned} |\Psi_0^L(t)\rangle &= e^{iF_0(t)} [\cos \frac{\chi^L(t)}{2} |a\rangle_L + \sin \frac{\chi^L(t)}{2} e^{i\xi^L(t)} |11\rangle_L], \\ |\Psi_1^L(t)\rangle &= e^{iF_1(t)} [\sin \frac{\chi^L(t)}{2} e^{-i\xi^L(t)} |a\rangle_L - \cos \frac{\chi^L(t)}{2} |11\rangle_L], \end{aligned}$$

under the control of $\mathcal{H}_{L_2}(t)$, similar to derivation process of Eq. (2) to Eq. (7), in addition to meeting geometric condition, we also need to determine parameter $\chi_1^L = 0$ to ensure that the evolution state $|\Psi_1^L(t)\rangle$ will not leak to the non-computational subspace at the final moment $t = \tau'$, and accumulate a geometric phase as $\gamma_g = -\xi_2^L(1 - \cos \chi_2^L)/2$ in the two-logical-qubit state $|11\rangle_L$, where defining $\xi_1^L = 0$ for simplicity. Therefore, by engineering the Hamiltonian parameters Ω_{L_2} and $\phi_{L_2}(t)$ in the time segments $t \in [0, \tau'_1]$, $[\tau'_1, \tau'_2]$ and $[\tau'_2, \tau']$ as

$$\begin{aligned} \Omega_{L_2}\tau'_1 &= \chi_2^L, & \phi_{L_2}(t) &= \frac{\pi}{2}, \\ \Omega_{L_2}(\tau'_2 - \tau'_1) &= 2\xi_2^L \sin(2\chi_2^L), & \phi_{L_2}(t) &= \pi + \frac{\Omega_{L_2}(t - \tau'_1)}{2 \sin(2\chi_2^L)}, \\ \Omega_{L_2}(\tau' - \tau'_2) &= \chi_2^L, & \phi_{L_2}(t) &= \xi_2^L - \frac{\pi}{2}, \end{aligned} \quad (\text{S5})$$

respectively, with $\Delta_{L_2} = 0$, $-\Omega_{L_2} \tan \chi_2^L$, 0, the final evolution operator within two-logical-qubit DFS S_2 is

$$U_{\text{CP}}^g(\zeta) = \text{diag}\{1, 1, e^{i\zeta}, 1\}, \quad (\text{S6})$$

in which $\zeta = -\gamma_g = \xi_2^L(1 - \cos \chi_2^L)/2$. Notice that, for the two-logical-qubit controlled-phase geometric gate $U_{\text{CP}}^g(\pi/2)$ with the target phase $\zeta = \pi/2$, parameter χ_2^L (or ξ_2^L) still has different choices to realized a same gate type at the final time $\tau' = 2[\chi_2^L + \xi_2^L \sin(2\chi_2^L)]/\Omega_{L_2}$, so we determine $\chi_2^L = 0.56\pi$ to gain the least gate-time consumption.

Appendix D: Quantum master equation and calculating fidelity

Quantum system is inevitably affected by decoherence due to its coupling with the surrounding environment, so we need to consider the effects of decoherence and the neglected high-order oscillating terms simultaneously in our subsequent numerical simulation. The performance of our universal logical-qubit gates can be numerically evaluated by using the quantum master equation as follows:

$$\dot{\rho}_n = -i[\mathcal{H}_I^n(t), \rho_n] + \sum_{n'=1}^n \sum_{u=-,z} \frac{\kappa_u^{n'}}{2} \mathcal{L}(X_u^{n'}) + \sum_{w=a,b} \frac{\kappa_w}{2} \mathcal{L}(Y_w), \quad (\text{S7})$$

where ρ_n is the density matrix of quantum system under consideration, $\mathcal{L}(\mathcal{A}) = 2\mathcal{A}\rho_n\mathcal{A}^\dagger - \mathcal{A}^\dagger\mathcal{A}\rho_n - \rho_n\mathcal{A}^\dagger\mathcal{A}$ is the Lindblad operator for operator \mathcal{A} with $X_-^n = \sum_{j=0}^{+\infty} \sqrt{j+1} |j\rangle_n \langle j+1|$, $X_z^n = \sum_{j=0}^{+\infty} j |j\rangle_n \langle j|$ and $Y_w = \sum_{j=0}^{+\infty} |j\rangle_w \langle j+1|$; κ_-^n and κ_z^n are the decay and dephasing rates of transmon T_n , and κ_w is the decay rate of microwave resonator R_w . $n=1$ and $n=2$ represent the single- and two-logical-qubit cases, respectively. Notice that, for the case of two-logical qubits, we consider the effects of the high-order oscillating terms and decoherence of all transmons (T_1 , T_2) and microwave resonators (R_a , R_b). Therefore, by numerically solving the above quantum master equation, we can obtain the final density matrices ρ_{f1} and ρ_{f2} of single qubit and two-logical qubits.

We next use the solved density matrix to fully evaluate our implemented geometric quantum gates based on DFS encoding. Thus we can define the gate fidelity of single-logical qubit as: $F_1^G = \frac{1}{2\pi} \int_0^{2\pi} \langle \psi_{f1} | \rho_{f1} | \psi_{f1} \rangle d\theta_1$, where $|\psi_{f1}\rangle = U(\tau) |\psi_1\rangle$ is the ideal final state for general initial state of single-logical qubit $|\psi_1\rangle = \cos \theta_1 |0\rangle_L + \sin \theta_1 |1\rangle_L$. In the same way, based on solved density matrix ρ_{f2} , two-logical-qubit gate fidelity can be defined as: $F_{\text{CP}}^G = \frac{1}{4\pi^2} \int_0^{2\pi} \int_0^{2\pi} \langle \psi_{f\text{CP}} | \rho_{f2} | \psi_{f\text{CP}} \rangle d\theta_1 d\theta_2$ where $|\psi_{f\text{CP}}\rangle = U_{\text{CP}}^g(\pi/2) |\psi_2\rangle$ is the ideal final state for general initial state of two-logical qubits $|\psi_2\rangle = (\cos \vartheta_1 |0\rangle_L + \sin \vartheta_1 |1\rangle_L) \otimes (\cos \vartheta_2 |0\rangle_L + \sin \vartheta_2 |1\rangle_L)$.

[1] M. A. Nielsen and I. L. Chuang, *Quantum Computation and Quantum Information* (Cambridge University Press, 2000).

[2] M. V. Berry, Quantal phase factors accompanying adiabatic changes, Proc. R. Soc. London A **392**, 45 (1984).

- [3] F. Wilczek and A. Zee, Appearance of gauge structure in simple dynamical systems, *Phys. Rev. Lett.* **52**, 2111 (1984).
- [4] Y. Aharonov and J. Anandan, Phase change during a cyclic quantum evolution, *Phys. Rev. Lett.* **58**, 1593 (1987).
- [5] J. Samuel and R. Bhandari, General Setting for Berry's Phase, *Phys. Rev. Lett.* **60**, 2339 (1988).
- [6] P. Zanardi and M. Rasetti, Holonomic quantum computation, *Phys. Lett. A* **264**, 94 (1999).
- [7] J. Pachos, P. Zanardi, and M. Rasetti, Non-Abelian Berry connections for quantum computation, *Phys. Rev. A* **61**, 010305(R) (1999).
- [8] J. A. Jones, V. Vedral, A. Ekert, and G. Castagnoli, Geometric quantum computation using nuclear magnetic resonance, *Nature* **403**, 869 (2000).
- [9] L.-M. Duan, J. I. Cirac, and P. Zoller, Geometric manipulation of trapped ions for quantum computation, *Science* **292**, 1695 (2001).
- [10] L. Faoro, J. Siewert, and R. Fazio, Non-Abelian Holonomies, Charge Pumping, and Quantum Computation with Josephson Junctions, *Phys. Rev. Lett.* **90**, 028301 (2003).
- [11] W. Xiang-Bin and M. Keiji, Nonadiabatic conditional geometric phase shift with NMR, *Phys. Rev. Lett.* **87**, 097901 (2001).
- [12] S.-L. Zhu and Z. D. Wang, Implementation of universal quantum gates based on nonadiabatic geometric phases, *Phys. Rev. Lett.* **89**, 097902 (2002).
- [13] S.-L. Zhu and Z. D. Wang, Unconventional geometric quantum computation, *Phys. Rev. Lett.* **91**, 187902 (2003).
- [14] E. Sjöqvist, D. M. Tong, L. M. Andersson, B. Hessmo, M. Johansson, and K. Singh, Non-adiabatic holonomic quantum computation, *New J. Phys.* **14**, 103035 (2012).
- [15] P. Z. Zhao, X. D. Cui, G. F. Xu, E. Sjöqvist, and D. M. Tong, Rydberg-atom-based scheme of nonadiabatic geometric quantum computation, *Phys. Rev. A* **96**, 052316 (2017).
- [16] T. Chen and Z.-Y. Xue, Nonadiabatic geometric quantum computation with parametrically coupled transmons, *Phys. Rev. Appl.* **10**, 054051 (2018).
- [17] W. Dong, F. Zhuang, S. E. Economou, and E. Barnes, Doubly Geometric Quantum Control, *PRX Quantum* **2**, 030333 (2021).
- [18] D. Leibfried *et al.*, Experimental demonstration of a robust, high-fidelity geometric two ion-qubit phase gate, *Nature (London)* **422**, 412 (2003).
- [19] M.-Z. Ai *et al.*, Experimental realization of nonadiabatic holonomic single-qubit quantum gates with optimal control in a trapped ion, *Phys. Rev. Appl.* **14**, 054062 (2020).
- [20] J. Du, P. Zou, and Z. D. Wang, Experimental implementation of high-fidelity unconventional geometric quantum gates using an NMR interferometer, *Phys. Rev. A* **74**, 020302(R) (2006).
- [21] G. Feng, G. Xu, and G. Long, Experimental realization of nonadiabatic holonomic quantum computation, *Phys. Rev. Lett.* **110**, 190501 (2013).
- [22] H. Li, Y. Liu, and G. Long, Experimental realization of single-shot nonadiabatic holonomic gates in nuclear spins, *Sci. China-Phys. Mech. Astron.* **60**, 080311 (2017).
- [23] Z. Zhu, T. Chen, X. Yang, J. Bian, Z.-Y. Xue, and X. Peng, Single-loop and composite-loop realization of nonadiabatic holonomic quantum gates in a decoherence-free subspace, *Phys. Rev. Appl.* **12**, 024024 (2019).
- [24] A. A. Abdumalikov, J. M. Fink, K. Juliusson, M. Pechal, S. Berger, A. Wallraff, and S. Filipp, Experimental realization of non-Abelian non-adiabatic geometric gates, *Nature (London)* **496**, 482 (2013).
- [25] Y. Xu *et al.*, Single-Loop Realization of Arbitrary Nonadiabatic Holonomic Single-Qubit Quantum Gates in a Superconducting Circuit, *Phys. Rev. Lett.* **121**, 110501 (2018).
- [26] D. J. Egger, M. Ganzhorn, G. Salis, A. Fuhrer, P. Müller, P. K. Barkoutsos, N. Moll, I. Tavernelli, and S. Filipp, Entanglement Generation in Superconducting Qubits Using Holonomic Operations, *Phys. Rev. Appl.* **11**, 014017 (2019).
- [27] T. Yan *et al.*, Experimental realization of nonadiabatic shortcut to non-Abelian geometric gates, *Phys. Rev. Lett.* **122**, 080501 (2019).
- [28] Y. Xu *et al.*, Experimental Implementation of Universal Nonadiabatic Geometric Quantum Gates in a Superconducting Circuit, *Phys. Rev. Lett.* **124**, 230503 (2020).
- [29] P. Z. Zhao, Z. Dong, Z. Zhang, G. Guo, D. M. Tong, and Y. Yin, Experimental realization of non-adiabatic geometric gates with a superconducting xmon qubit, *Sci. China-Phys. Mech. Astron.* **64**, 250362 (2021).
- [30] K. Xu, W. Ning, X.-J. Huang, P.-R. Han, H. Li, Z.-B. Yang, D. Zheng, H. Fan, and S.-B. Zheng, Demonstration of a non-Abelian geometric controlled-NOT gate in a superconducting circuit, *Optica* **8**, 972 (2021).
- [31] C. Zu, W.-B. Wang, L. He, W.-G. Zhang, C.-Y. Dai, F. Wang, and L.-M. Duan, Experimental realization of universal geometric quantum gates with solid-state spins, *Nature (London)* **514**, 72 (2014).
- [32] S. Arroyo-Camejo, A. Lazariev, S. W. Hell, and G. Balasubramanian, Room temperature high-fidelity holonomic single-qubit gate on a solid-state spin, *Nat. Commun.* **5**, 4870 (2014).
- [33] Y. Sekiguchi, N. Niikura, R. Kuroiwa, H. Kano, and H. Kosaka, Optical holonomic single quantum gates with a geometric spin under a zero field, *Nat. Photonics* **11**, 309 (2017).
- [34] B. B. Zhou, P. C. Jerger, V. O. Shkolnikov, F. J. Heremans, G. Burkard, and D. D. Awschalom, Holonomic Quantum Control by Coherent Optical Excitation in Diamond, *Phys. Rev. Lett.* **119**, 140503 (2017).
- [35] K. Nagata, K. Kuramitani, Y. Sekiguchi, and H. Kosaka, Universal holonomic quantum gates over geometric spin qubits with polarised microwaves, *Nat. Commun.* **9**, 3227 (2018).
- [36] Y. Dong *et al.*, Experimental implementation of universal holonomic quantum computation on solid-state spins with optimal control, *Phys. Rev. Appl.* **16**, 024060 (2021).
- [37] Y. Ota and Y. Kondo, Composite pulses in NMR as nonadiabatic geometric quantum gates, *Phys. Rev. A* **80**, 024302 (2009).
- [38] J. Zhou, S. Li, G.-Z. Pan, G. Zhang, T. Chen, and Z.-Y. Xue, Nonadiabatic geometric quantum gates that are insensitive to qubit-frequency drifts, *Phys. Rev. A* **103**, 032609 (2021).
- [39] G. F. Xu and G. L. Long, Protecting geometric gates by dynamical decoupling, *Phys. Rev. A* **90**, 022323 (2014).
- [40] X. Wu and P. Z. Zhao, Universal nonadiabatic geometric gates protected by dynamical decoupling, *Phys. Rev. A* **102**, 032627 (2020).
- [41] T. Chen and Z.-Y. Xue, High-Fidelity and Robust Geometric Quantum Gates that Outperform Dynamical Ones, *Phys. Rev. Appl.* **14**, 064009 (2020).
- [42] C.-Y. Ding, L.-N. Ji, T. Chen, and Z.-Y. Xue, Path-optimized nonadiabatic geometric quantum computation on superconducting qubits, *Quantum Sci. Technol.* **7**, 015012 (2022).
- [43] L. A. Wu, P. Zanardi, and D. A. Lidar, Holonomic Quantum Computation in Decoherence-Free Subspaces, *Phys. Rev. Lett.* **95**, 130501 (2005).
- [44] L. X. Cen, Z. D. Wang, and S. J. Wang, Scalable quantum computation in decoherence-free subspaces with trapped ions, *Phys. Rev. A* **74**, 032321 (2006).
- [45] X. L. Feng, C. F. Wu, H. Sun, and C. H. Oh, Geometric Entangling Gates in Decoherence-Free Subspaces with Minimal Requirements, *Phys. Rev. Lett.* **103**, 200501 (2009).

[46] G. F. Xu, J. Zhang, D. M. Tong, E. Sjöqvist, and L. C. Kwek, Nonadiabatic holonomic quantum computation in decoherence-free subspaces, *Phys. Rev. Lett.* **109**, 170501 (2012).

[47] J. Zhang, L.-C. Kwek, E. Sjöqvist, D. M. Tong, and P. Zanardi, Quantum computation in noiseless subsystems with fast non-Abelian holonomies, *Phys. Rev. A* **89**, 042302 (2014).

[48] Z.-Y. Xue, J. Zhou, and Z. D. Wang, Universal holonomic quantum gates in decoherence-free subspace on superconducting circuits, *Phys. Rev. A* **92**, 022320 (2015).

[49] P. Z. Zhao, G. F. Xu, and D. M. Tong, Nonadiabatic geometric quantum computation in decoherence-free subspaces based on unconventional geometric phases, *Phys. Rev. A* **94**, 062327 (2016).

[50] T. Chen, P. Shen, and Z.-Y. Xue, Robust and Fast Holonomic Quantum Gates with Encoding on Superconducting Circuits, *Phys. Rev. Appl.* **14**, 034038 (2020).

[51] L.-M. Duan and G.-C. Guo, Preserving coherence in quantum computation by pairing quantum bits, *Phys. Rev. Lett.* **79**, 1953 (1997).

[52] P. Zanardi and M. Rasetti, Noiseless quantum codes, *Phys. Rev. Lett.* **79**, 3306 (1997).

[53] D. A. Lidar, I. L. Chuang, and K. B. Whaley, Decoherence-free subspaces for quantum computation, *Phys. Rev. Lett.* **81**, 2594 (1998).

[54] P. G. Kwiat, A. J. Berglund, J. B. Altepeter, and A. G. White, Experimental Verification of Decoherence-Free Subspaces, *Science* **290**, 498 (2000).

[55] F. Motzoi, J. M. Gambetta, P. Rebentrost, and F. K. Wilhelm, Simple Pulses for Elimination of Leakage in Weakly Nonlinear Qubits, *Phys. Rev. Lett.* **103**, 110501 (2009).

[56] Z. Chen *et al.*, Measuring and suppressing quantum state leakage in a superconducting qubit, *Phys. Rev. Lett.* **116**, 020501 (2016).

[57] J. D. Strand, M. Ware, F. Beaudoin, T. A. Ohki, B. R. Johnson, A. Blais, and B. L. T. Plourde, First-order sideband transitions with flux-driven asymmetric transmon qubits, *Phys. Rev. B* **87**, 220505 (2013).

[58] M. Reagor *et al.*, Demonstration of universal parametric entangling gates on a multi-qubit lattice, *Sci. Adv.* **4**, eaao3603 (2018).

[59] R. W. Heeres, P. Reinhold, N. Ofek, L. Frunzio, L. Jiang, M. H. Devoret, and R. J. Schoelkopf, Implementing a universal gate set on a logical qubit encoded in an oscillator, *Nat. Commun.* **8**, 94 (2017).

[60] R. Barends *et al.*, Superconducting quantum circuits at the surface code threshold for fault tolerance, *Nature (London)* **508**, 500 (2014).

[61] S.-B. Zheng, C.-P. Yang, and F. Nori, Comparison of the sensitivity to systematic errors between nonadiabatic non-Abelian geometric gates and their dynamical counterparts, *Phys. Rev. A* **93**, 032313 (2016).